Icarus 434 (2025) 116544

Contents lists available at ScienceDirect

Icarus

journal homepage: www.elsevier.com/locate/icarus

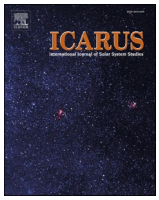

The effects of measured slope on Martian lava flow modeling

Frances P. Russo [a], Ian T.W. Flynn [a,*], Sean I. Peters [b], Michael S. Ramsey [a]

[a] Department of Geology and Environmental Science, University of Pittsburgh, Pittsburgh, PA 15260, United States of America
[b] Department of Earth and Climate Sciences, Middlebury College, Middlebury, VT 05753, United States of America

ARTICLE INFO

Keywords:
Lava flows
Topography
Mars
Volcanology
Rheology

ABSTRACT

One of the most frequently used methods for modeling lava flows on Mars is commonly called the "standard rheologic approach" (SRA). This method requires measurements of the flow dimensions (e.g., width, length, thickness) and local topography (e.g., slope), which are used in equations of viscosity and yield strength, for example. Topography is a critical input for most lava flow models, a detailed analysis of how the input slope value affects the results using the SRA is needed. Here we present a topographic sensitivity analysis of SRA modeling, using the minimum, maximum, and one standard deviation of measured slope values. We investigated sixteen lava flows, fourteen south and two north of Arsia Mons, Mars. Depending on the input slope, a 5 % to 60 % change in viscosity, and a 5 % to 70 % change in yield strength was found. This viscosity range produced an inferred composition change from a basalt to an andesite for eight of the sixteen flows. We also tested a single flow using the SRA and derived slopes from MOLA, HRSC, and CTX digital elevation models (DEMs). The same compositional shift from a basalt to an andesite occurred with increasing DEM resolution. These results highlight the importance of testing the full range of possible slopes and using the highest resolution topographic dataset available to avoid inaccurate interpretation of flow composition. If only low to moderate DEM datasets are available, the results should be interpreted with caution.

1. Introduction

The surface of Mars is covered with a diverse range of lava flow textures and morphologies (Bleacher et al., 2007; Carr, 1973; Mouginis-Mark and Yoshioka, 1998; Zimbelman et al., 2015). Many lava flows within the Tharsis and Elysium volcanic provinces have been investigated using a combination of detailed morphologic studies (Bleacher et al., 2007; Crown and Ramsey, 2017; Voigt et al., 2023), analog investigations (Peitersen and Crown, 1999; Ramsey et al., 2016; Theilig and Greeley, 1986), and a variety of numerical models (Baloga and Glaze, 2008; Flynn et al., 2022; Peters et al., 2021). Understanding the emplacement of Martian lava flows provides insight into their rheology, eruption dynamics, and magmatic evolution.

A frequently used method for investigating lava flows on Mars is the "standard rheologic approach" (SRA). The SRA utilizes the Graetz number – a dimensionless value characterizing laminar flow in a conduit – to calculate effusion rate. It also uses the Jeffreys equation – derived for the flow of water and thus assuming a Newtonian rheology – to calculate viscosity. The application of the SRA to Martian lava flows was initially presented in Hiesinger et al. (2007) for investigating lava flows on the flanks of Ascraeus Mons. It was later applied to flows across the Tharsis volcanic province (Peters et al., 2021), Elysium Mons (Pasckert et al., 2012), and Alba Mons (Wiedeking et al., 2022). Although the method has been widely adopted, more recent studies evaluated the impact of possible input parameters on the SRA output. For example, Peters et al. (2021) highlighted how variations in the assumed Graetz number can cause ~19 % to ~30 % differences in the modeled eruption rate and viscosity. Wiedeking et al. (2022) applied the method to lava flows on Alba Mons and determined error ranges for ±10 %, ±30 %, and ± 50 % for measured flow parameters (thickness, width, length), density, thermal diffusivity, and slope. Furthermore, the SRA use of measured flow dimensions implicitly assumes the entire lava flow is active during emplacement, an assumption that is refuted by observations of active lava flows, which tend to have mobile lava concentrated into a discrete area (e.g., a channel) relative to the entire area of active flow. Although this method can produce results with a large range of uncertainty, it is still the most commonly used method to investigate the emplacement and rheology of Martian lava flows. Thus, constraining the effects of model inputs on results can help increase their interpretation and accuracy.

* Corresponding author.
E-mail address: itf2@pitt.edu (I.T.W. Flynn).

https://doi.org/10.1016/j.icarus.2025.116544
Received 13 November 2024; Received in revised form 13 February 2025; Accepted 4 March 2025
Available online 7 March 2025

A critical input for nearly all lava flow models is the underlying topography; however, a detailed statistical analysis of how it affects the SRA results has not been performed. Previous studies have noted the importance of accurate topography and dataset resolution for planetary lava flow modeling (e.g., Flynn et al., 2023; Glaze and Baloga, 2007). For this study, we present a focused analysis of how variations in the input slope can affect the calculated SRA results. We also suggest ways to account for these discrepancies in future studies.

1.1. Study region

Our study region focuses on the channelized lava flows within the flow fields north and south of Arsia Mons. Arsia Mons is the southernmost of the Tharsis Montes (Fig. 1). The volcano is primarily constructed through overlapping layers of lava flows, with some evidence of pyroclastic layering within the flanks and caldera (Mouginis-Mark and Rowland, 2008; Ganesh et al., 2020). The central caldera contains numerous small vents, with activity in the caldera occurring as recently as 10–90 Ma (Richardson et al., 2017).

To the northeast and southwest of the main volcano, two large flow fields emanate from the flanks. Both flow fields have been dated as Amazonian (Tanaka et al., 2014), with specific groups of flows (22.5°–27.5°S and 120°–130°W) south of Arsia Mons having estimated ages of only a few 100 Ma (Berman and Crown, 2019; Crown et al., 2015). This suggests these flows are some of the youngest on Mars. In addition to the relative age dating of lava flows in the southern field, detailed morphologic and modeling studies have also been performed (e.g., Crown and Ramsey, 2017; Flynn et al., 2022). Regional studies of the field north of Arsia Mons have identified flows with ages between 100 and 800 My (Werner, 2009). However, similar detailed age, modeling, and morphology studies of these lava flows have not been performed.

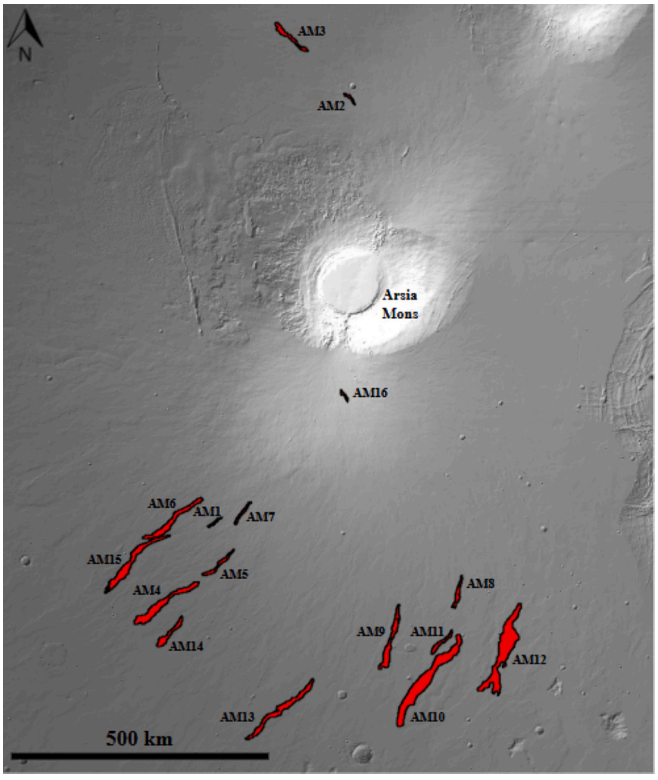

Fig. 1. Hillshade image derived from Mars Orbital Laser Altimeter (MOLA) data of the study area – Arsia Mons and surrounding plains – located in the Tharsis Province on Mars. The lava flows modeled in this study (outlined in red) are located in flow fields to the north and south of Arsia Mons. (For interpretation of the references to colour in this figure legend, the reader is referred to the web version of this article.)

2. Materials and methods

2.1. Flow measurements

For this investigation, we limited our study to channelized lava flows, defined as having a distinct, observable central channel; and adjacent near-parallel constructed levees. Channelized flows represent a narrow range of emplacement conditions (Gregg, 2017 and references therein). Specifically, this flow morphology is indicative of higher effusion rates, earlier formation during a new eruption, and a sustained effusive period (e.g., Gregg and Fink, 2000; Kerr et al., 2006; Rowland et al., 2005).

The detailed measurements of flow dimensions followed methods described in Flynn et al. (2022). The length of each flow was measured from a profile drawn down the line of maximum descent (e.g., the thalweg) using data from the Context Camera (CTX) (~6 m/pixel) (Malin et al., 2007). Measurements for channel and total flow width were performed every 1000 m along this length (Fig. 2). Flow thickness was calculated using the Mars Orbiting Laser Altimeter (MOLA) Precision Experimental Data Record (PEDR) data (~160 m spot size, ~300 m along track spacing and 37 cm effective vertical resolution) (Smith et al., 2003) by taking a transect adjacent to, and another along, the central flow channel (Fig. 2). Local slope was then retrieved from the MOLA/High Resolution Stereo Camera (HRSC) (~200 m/pixel; ± 3 m vertical resolution) blended Digital Elevation Model (DEM) (Fergason et al., 2018), by taking a profile adjacent to each flow (Fig. 2). Each of these slope profiles ran the entire observable length of the lava flow. All flow measurements were performed in the Java Mission-planning and Analysis for Remote Sensing (JMARS) software and ArcGIS Pro.

2.2. Standard rheologic approach (SRA)

Each lava flow was modeled following the SRA as described in Hiesinger et al. (2007). This approach uses the Graetz number to first calculate the average effusion rate of an eruption, which in turn is used with the Jeffrey's equation to calculate viscosity. The Graetz number is a dimensionless value for characterizing laminar lava flows, originally described by Wilson and Head (1983). A Graetz value of 300 is the generally agreed upon value of flow cessation due to crust extent and strength (Pinkerton and Sparks, 1976). The equations used in the SRA modeling approach are described below.

The Graetz number (G_z) equation is used to first calculate effusion rate (Q):

$$Q = G_z k x w / h \tag{1}$$

Jeffrey's equation is next used to calculate the effective dynamic viscosity (η) with the effusion rate calculated in Eq. (1):

$$\eta = \rho g h^3 w \sin(\alpha) / 3Q \tag{2}$$

Yield strength (T) is defined as:

$$T = \rho g \sin(\alpha) h \tag{3}$$

Constants used in these equations include: k, the thermal diffusivity (5×10^{-7} m^2/s); G_z, the predetermined Graetz number (300); ρ, the lava density (2700 kg/m^3); and g, gravitational acceleration (3.7 m/s^2). These were chosen based on terrestrial values and prior studies (e.g., Hiesinger et al., 2007; Peters et al., 2021). The input variables for each flow are the measured slope (α), average total flow width (w), average flow thickness (h), and flow length (x).

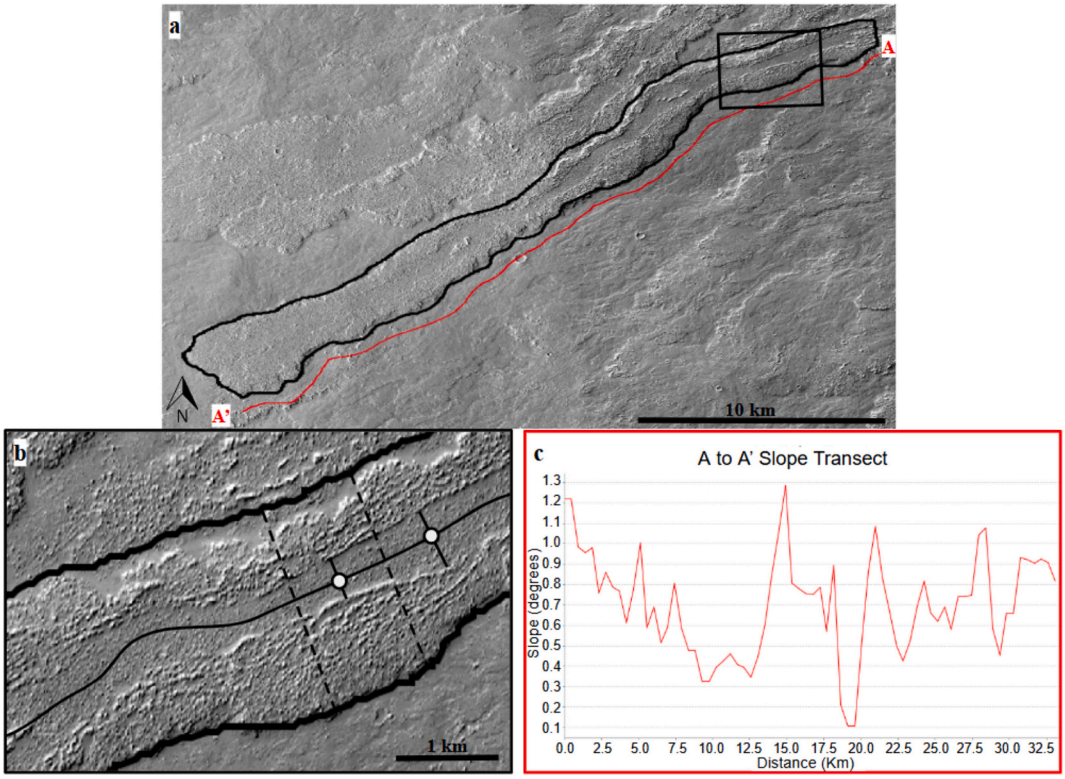

Fig. 2. (a) CTX image showing the AM1 flow outlined in black, with the red line indicating the slope profile from A to A' shown in (c). The black rectangle highlights the area shown in (b). (b) A region of the lava flow showing the central channel marked by the solid black line, example measurement points as white circles, example central channel width measurements as solid black lines through those circles, and total width measurements as black dashed lines. (c) Profile of the slope transect taken adjacent to the lava flow, running from A to A' (start of the flow to termination of the flow). (For interpretation of the references to colour in this figure legend, the reader is referred to the web version of this article.)

2.3. Slope variations

To quantify the impact of slope variability on the SRA, we varied the average input slope values. This was the only variable (slope) modified, with the remaining left constant, to observe the impact of slope directly. We used the average slope, minimum, maximum, and ± one standard deviation (±1σ) of the average slope, calculated utilizing the full slope transect data. The various slope values were then incorporated into the SRA modeling for each flow investigated. Previous SRA studies (e.g., Pasckert et al., 2012; Wiedeking et al., 2022) have used ±10 %, ±30 %, ±50 %, and/or ± 70 % of the averaged measured slope value (e.g., Pasckert et al., 2012; Wiedeking et al., 2022). We also test the ±10 % and ± 50 %values to assess whether they result in an accurate representation of the measured slope values.

3. Results

We measured flow dimensions for sixteen lava flows, fourteen on the southern flank and two on the northern flank of Arsia Mons (Fig. 1). Each has a well developed central channel with flow textures and morphology similar to the channelized flows described in Crown and Ramsey (2017) and Flynn et al. (2022). The measured flow dimensions include the observable length, average full width, average thickness, and slope statistics (Tables 1 and 2). In the following sections, we report the calculated effusion rates, viscosity, yield strength, and how variations in slope values affect the SRA model results.

3.1. Effusion rate

Calculated effusion rate values for each lava flow are summarized in Table 3. The effusion rates for the sixteen flows ranged from 9.9×10^1 to 1.6×10^4 m^3/s, with an average of 3.7×10^3 m^3/s. The effusion rates increased in relation to their observable flow length as one would expect. Flow AM16 is the shortest (25 km) with one of the smallest modeled effusion rates (2.5×10^2 m^3/s), whereas AM11 is 2.7×10^2 km long resulting in a calculated effusion rate of 1.6×10^4 m^3/s. These effusion rates are comparable to those determined using the same SRA method for flows at Elysium Mons (Pasckert et al., 2012) and are higher than those calculated at Alba and Ascreaus Mons (Hiesinger et al., 2007; Wiedeking et al., 2022). The calculated effusion rates for a single Martian lava flow are also much higher than those for recent terrestrial eruptions. For example, the 2007 and 2010 eruptions of Piton de la Fournaise volcano had effusion rate peaks as high as ~200 and ~ 130 m^3/s, respectively (Soldati et al., 2018; Staudacher et al., 2009), and the 2021 Fagradalsfjall eruption in Iceland had a maximum of only 13 m^3/s (Pedersen et al., 2022).

3.2. Viscosity

The modeled viscosity values had a broader distribution than the effusion rates, ranging from 10^4 to 10^7 Pa s (Table 3). A lower average flow thickness correlated to lower viscosities, with flows under 20 m thick (e.g., AM5, AM7, AM13, AM14, and AM15) all having viscosities of $>10^6$ Pa s. In contrast, flows over 40 m thick (e.g., AM2, AM10, and AM16) had modeled viscosities of 10^7 Pa s (Table 3). The calculated viscosities are similar to those determined in previous studies, using the same method, for other volcanic regions on Mars (Pasckert et al., 2012; Peters et al., 2021; Wiedeking et al., 2022). Basaltic lava flows from the western volcanic zone in Iceland had a viscosity of 10^5 Pa s (Chevrel et al., 2013) and the 2018 Kilauea eruption ranged from 10^3 to 10^6 Pa s (Gansecki et al., 2019), similar to the results found in this study. Terrestrial basaltic trachyandesite lava from the 2012–2013 Tolbachik

Table 1
Measured values for the analyzed lava flows surrounding Arsia Mons. *Indicates lava flows studied by Peters et al., 2021.

Flow Number	Coordinates	Flow Length (km)	Avg. Flow Width (m)	Avg. Flow Thickness (m)	Avg. Slope (°)
AM1	−16.996°N, 235.287°E	63	2690	27	0.45
AM2	−3.12°N, 239.621°E	39	2759	41	0.58
AM3	−1.076°N, 237.803°E	103	5777	27	0.44
AM4	−19.896°N, 233.174°E	127	6448	26	0.21
AM5	−18.395°N, 234.928°E	52	4201	17	0.44
AM6	−16.951°N, 233.943°E	127	4580	44	0.37
AM7	−16.723°N, 235.895°E	44	3006	12	0.37
AM8*	−19.332°N, 243.262°E	78	5900	25	0.24
AM9*	−20.945°N, 240.957°E	137	16,300	36	0.56
AM10*	−21.733°N, 242.555°E	58	19,300	45	0.71
AM11*	−23.297°N, 242.812°E	266	11,800	30	0.28
AM12*	−22.547°N, 244.16°E	201	6000	32	0.32
AM13*	−23.195°N, 237.617°E	219	3800	15	0.28
AM14*	−19.081°N, 234.684°E	92	3200	16	0.36
AM15*	−17.307°N, 233.48°E	165	4500	17	0.23
AM16*	−12.934°N, 239.423°E	25	2100	31	1.34

Table 2
Measured values for the analyzed lava flows surrounding Arsia Mons, used to observe how variations in slope and flow width impact the modeling results.

Flow Number	Min. Slope (°)	Max. Slope (°)	σSlope (°)	10 % of average slope	50 % of average slope
AM1	0.14	0.99	0.15	0.05	0.23
AM2	0.05	1.38	0.23	0.06	0.29
AM3	0.03	2.66	0.33	0.04	0.22
AM4	0.00	1.37	0.15	0.02	0.11
AM5	0.05	0.84	0.14	0.04	0.22
AM6	0.03	0.83	0.15	0.04	0.19
AM7	0.08	0.68	0.12	0.04	0.19
AM8	0.05	0.57	0.10	0.02	0.12
AM9	0.07	1.51	0.30	0.06	0.28
AM10	0.07	2.30	0.41	0.07	0.36
AM11	0.04	1.31	0.17	0.03	0.14
AM12	0.03	1.63	0.23	0.03	0.16
AM13	0.05	1.35	0.19	0.03	0.14
AM14	0.03	6.33	0.74	0.04	0.18
AM15	0.03	0.70	0.12	0.02	0.12
AM16	0.25	4.02	0.80	0.13	0.67

eruption, however, had a higher viscosity (10^5 to 10^7 Pa s) for the 'a'a lava fronts (Belousov and Belousova, 2017).

3.3. Yield strength

Yield strength values ranged from 6.9×10^2 to 7.3×10^3 Pa (Table 3). Flow AM16 had the largest yield strength calculated. Similar to the calculated viscosities, the yield strength values for each flow are comparable to those determined in previous studies, using the same method, for other volcanic regions on Mars (Pasckert et al., 2012; Peters et al., 2021; Wiedeking et al., 2022). These calculated values are also comparable to those for terrestrial basaltic lava flows in Iceland's western volcanic zone (2.1 to 4.7 × 10^3 Pa) (Chevrel et al., 2018), the 2014–2015 Holuhraun eruption (3.16 to 2.5 × 10^3 Pa) in Iceland (Kolzenburg et al., 2018), and at Mt. Etna, Italy (280 to 590 Pa) (Sparks et al., 1976).

Table 3
Results for each lava flow using the SRA with an average slope value for each lava flow.

Flow Number	Effusion Rate (m^3/s)	Viscosity (Pa s)	Yield Strength (Pa)
AM1	9.6×10^2	1.4×10^6	2.1×10^3
AM2	9.9×10^1	1.6×10^7	4.2×10^3
AM3	4.9×10^2	9.3×10^5	2.1×10^3
AM4	7.4×10^2	3.1×10^5	9.8×10^2
AM5	5.4×10^2	2.7×10^5	1.3×10^3
AM6	4.9×10^2	4.1×10^6	2.8×10^3
AM7	5.6×10^2	7.7×10^4	8.0×10^2
AM8	2.8×10^3	4.6×10^5	1.0×10^3
AM9	9.4×10^3	2.5×10^6	3.5×10^3
AM10	3.7×10^3	1.9×10^7	5.5×10^3
AM11	1.6×10^4	3.3×10^5	1.5×10^3
AM12	5.7×10^3	6.5×10^5	1.8×10^3
AM13	8.3×10^3	2.5×10^4	7.4×10^2
AM14	2.8×10^3	1.0×10^5	1.0×10^3
AM15	6.6×10^3	4.5×10^4	6.9×10^2
AM16	2.5×10^2	1.9×10^7	7.3×10^3

3.4. Slope variations on the SRA

Slope statistics for each flow are compiled in Table 2. The SRA results using the minimum, maximum and ± 1σ for slope, are summarized in Table 4, and the results using ±10 % and ± 50 % for slope are summarized in Table 5. The viscosity and yield strength values calculated using the minimum and maximum slopes were on average ± 50 % of those calculated using the average slope. In addition, viscosity and yield strength values calculated using ±1σ of the average slope resulted in a ± 30 % change. A difference of 20 % and 15 % was calculated between the standard deviation and the 10 % and 50 % of the average slope, respectively. This indicates that the 50 % error range used in previous studies (i.e., Wiedeking et al., 2022) provides a more realistic range of the measured slope values than the ±10 % and ± 30 % of the average slope.

The calculated viscosities for the minimum and maximum slope values for any given flow ranged from 0 to 6.3×10^7 Pa s. One flow (e.g., AM14) had a three order of magnitude variation in viscosity, whereas five lava flows (e.g., AM3, AM11, AM12, AM13, and AM15) had a two order of magnitude change, and the remaining eight had only a single order of magnitude change in viscosity. The variations in calculated viscosities using the standard deviation were smaller, with a distribution between 7.9×10^3 and 3.1×10^7 Pa s, with an average of 20 % change compared to using the average slope value, but values ranged from 5 % to 60 %. Whereas the lower range of viscosity (10^3 to 10^5 Pa s) still indicates a basaltic composition, the upper range (10^6 to 10^7 Pa s) is more reasonable for an andesite (e.g., Cigolini et al., 1984; Murase and McBirney, 1973; Vetere et al., 2006).

Yield strength values from the minimum and maximum slopes ranged from 0 Pa to 1.2×10^4 Pa. The flows that exhibited the greatest change in yield strength were AM3, AM10, AM14, and AM16. These flows have lengths between 25 km to 103 km, average flow widths between 3200 m to 19,300 m, and average flow thicknesses between 16 m to 45 m. The flow exhibiting the least change was AM7, with an observable flow length of 44 km, an average flow width of 3006 m, and an average flow thickness of 12.4 m. AM3 is the only lava flow that exhibited higher changes in both viscosity and yield strength where the slope was varied. The variations in calculated yield strengths using the standard deviation resulted in an average 30 % change compared to

Table 4
Modeled values for viscosity and yield strength for the analyzed lava flows using the SRA with slope as a variable. Minimum and maximum standard deviation (σ) represent the results where the standard deviation of the slope was subtracted and added to the average, respectively. Min and Max represent the results of using the minimum and maximum values of slope.

Flow Number	Min. St. Dev. Viscosity (Pa s)	Max. St. Dev. Viscosity (Pa s)	Min. Viscosity (Pa s)	Max. Viscosity (Pa s)	Min. σ Yield Strength (Pa)	Max. σ Yield Strength (Pa)	Min. Yield Strength (Pa)	Max. Yield Strength (Pa)
AM1	9.5×10^5	1.9×10^6	4.4×10^5	3.1×10^6	1.4×10^3	2.8×10^3	6.5×10^2	4.6×10^3
AM2	9.9×10^6	2.3×10^7	1.4×10^6	3.9×10^7	2.5×10^3	5.8×10^3	3.4×10^2	9.9×10^3
AM3	2.4×10^5	1.6×10^6	7.2×10^4	5.7×10^6	5.5×10^2	3.7×10^3	1.6×10^2	1.3×10^4
AM4	8.7×10^4	5.4×10^5	0	2.0×10^6	2.7×10^2	1.7×10^3	0	6.3×10^3
AM5	1.8×10^5	3.6×10^5	3.3×10^4	5.2×10^5	8.6×10^2	1.7×10^3	1.6×10^2	2.5×10^3
AM6	2.4×10^6	5.7×10^6	2.8×10^5	9.1×10^6	1.7×10^3	3.9×10^3	1.9×10^2	6.3×10^3
AM7	5.2×10^4	1.0×10^5	1.6×10^4	1.4×10^5	5.4×10^2	1.1×10^3	1.6×10^2	1.5×10^3
AM8	2.7×10^5	6.5×10^5	1.0×10^5	1.1×10^6	6.1×10^2	1.5×10^3	2.3×10^2	2.5×10^3
AM9	1.2×10^6	3.9×10^6	3.0×10^5	6.8×10^6	1.7×10^3	5.3×10^3	4.2×10^2	9.3×10^3
AM10	8.2×10^6	3.0×10^7	2.0×10^6	6.3×10^7	2.4×10^3	8.7×10^3	5.7×10^2	1.8×10^4
AM11	6.5×10^4	5.4×10^5	5.0×10^4	1.5×10^6	2.9×10^2	2.4×10^3	2.2×10^2	6.8×10^3
AM12	1.8×10^5	1.1×10^6	6.9×10^4	3.3×10^6	5.0×10^2	3.1×10^3	1.9×10^2	9.1×10^3
AM13	7.9×10^3	4.3×10^4	4.1×10^3	1.2×10^5	2.3×10^2	1.2×10^3	1.2×10^2	3.5×10^3
AM14	1.1×10^5	3.0×10^5	9.4×10^3	1.7×10^6	1.1×10^3	3.0×10^3	9.5×10^1	1.8×10^4
AM15	2.3×10^4	6.8×10^4	6.7×10^3	1.4×10^5	3.4×10^2	1.0×10^3	1.0×10^2	2.1×10^3
AM16	7.7×10^6	3.1×10^7	3.5×10^6	5.8×10^7	2.9×10^3	1.2×10^4	1.3×10^3	2.2×10^4

Table 5
Modeled values for viscosity and yield strength utilizing slope values of ±10 % and ± 50 %.

Flow Number	Viscosity Slope + 10 % (Pa s)	Yield Strength Slope + 10 % (Pa)	Viscosity Slope − 10 % (Pa s)	Yield Strength Slope − 10 % (Pa)	Viscosity Slope + 50 % (Pa s)	Yield Strength Slope + 50 % (Pa)	Viscosity Slope − 50 % (Pa s)	Yield Strength Slope − 50 % (Pa)
AM1	1.6×10^6	2.3×10^3	1.3×10^6	1.9×10^3	2.1×10^6	3.2×10^3	7.1×10^5	1.1×10^3
AM2	1.8×10^7	4.6×10^3	1.5×10^7	3.7×10^3	2.4×10^7	6.2×10^3	8.1×10^6	2.1×10^3
AM3	1.0×10^6	2.3×10^3	8.4×10^5	1.9×10^3	1.4×10^6	3.2×10^3	4.7×10^5	1.1×10^3
AM4	3.4×10^5	1.1×10^3	2.8×10^5	8.7×10^2	4.7×10^5	1.6×10^3	1.6×10^5	4.8×10^2
AM5	3.0×10^5	1.4×10^3	2.5×10^5	1.2×10^3	4.1×10^5	2.0×10^3	1.4×10^5	6.5×10^2
AM6	4.5×10^6	3.1×10^3	3.7×10^6	2.5×10^3	6.1×10^6	4.2×10^3	2.0×10^6	1.4×10^3
AM7	8.5×10^4	8.8×10^2	6.9×10^4	7.2×10^2	1.2×10^5	1.2×10^3	3.9×10^4	4.0×10^2
AM8	5.1×10^5	1.2×10^3	4.2×10^5	9.4×10^2	7.0×10^5	1.6×10^3	2.3×10^5	5.2×10^2
AM9	2.8×10^6	3.8×10^3	2.3×10^6	3.1×10^3	3.8×10^6	5.2×10^3	1.3×10^6	1.7×10^3
AM10	2.1×10^7	6.1×10^3	1.8×10^7	5.0×10^3	2.9×10^7	8.4×10^3	9.7×10^6	2.8×10^3
AM11	3.6×10^5	1.6×10^3	3.0×10^5	1.3×10^3	5.0×10^5	2.2×10^3	1.7×10^5	7.3×10^2
AM12	7.1×10^5	2.0×10^3	5.8×10^5	1.6×10^3	9.7×10^5	2.7×10^3	4.6×10^5	1.3×10^3
AM13	2.8×10^4	8.1×10^2	2.3×10^4	6.6×10^3	3.8×10^4	1.1×10^3	1.3×10^4	3.7×10^2
AM14	1.1×10^5	1.1×10^3	8.9×10^4	9.0×10^2	1.5×10^5	1.5×10^3	5.0×10^4	5.0×10^2
AM15	5.0×10^4	7.5×10^2	4.1×10^4	6.1×10^2	6.8×10^4	1.0×10^3	2.3×10^4	3.4×10^2
AM16	2.1×10^7	8.0×10^3	1.7×10^7	6.5×10^3	2.9×10^7	1.1×10^4	9.6×10^6	3.6×10^3

using the average slope value, with values ranging from 5 % to 70 % change.

4. Discussion

The results show that the slope value used in SRA modeling can produce a one to three-order magnitude change in the calculated viscosity and yield strength, which can result in an inaccurate derived composition. Given the limitations of Mars topographic datasets and the established effect that lower resolution topographic data has on derived slope value (Chang and Tsai, 1991; Evans, 1980; Flynn et al., 2023), these results are significant for any application of the SRA to modeling lava flows.

4.1. Interpreting SRA results

Warner and Gregg (2003) noted the importance of exercising caution in interpreting planetary rheologic modeling results. As prior studies indicate (Pasckert et al., 2012; Peters et al., 2021; Wiedeking et al., 2022) and confirmed here, assumptions made for model inputs can have a substantial effect on model outputs. The results of the SRA modeling (e.g., effusion rate, viscosity, and yield strength) rely on accurate flow dimension and underlying topography measurements.

Terrestrial eruptions do not have a constant effusion rate, and there is no evidence that Martian eruptions behave any differently (e.g., Pinkerton, 1987; Belousov and Belousova, 2017; Bonny and Wright, 2017). The SRA models a single effusion rate for the entire duration of an eruption, which is not accurate. Direct measurements of terrestrial eruptions show that effusion rate is highly variable throughout the eruption duration, usually starting high followed by an exponential decay with short-term variability caused by a variety of factors (e.g., Wadge, 1981; Harris et al., 2000; Ramsey et al., 2019; Voigt et al., 2022). In addition, the SRA assumes the entire lava flow is active during emplacement; however, field observations show that with time only a small portion of a flow (e.g., a central channel) is actually mobile with flow margins that remain relatively stationary (e.g., Baloga and Glaze, 2008). These assumptions can lead to an overestimation of calculated effusion rates.

Jeffrey's equation (Eq. (2)), modified to determine viscosity, utilizes the calculated effusion rate from the Graetz equation as well as an average slope value across the length of the exposed lava flow. Terrestrial lava flows cool and increase crystallinity as they propagate away from the vent, which results in an exponential increase in viscosity. We expect Martian flows to behave in a similar manner given their observed composition and environmental conditions. Jeffrey's equation also assumes Newtonian fluid behavior, and although this may be true for the

interior core of a flow, it is not the case for the cooler, more rigid flow exterior. Therefore, it has been proposed that an entire lava flow may behave as a Bingham plastic, which has a yield strength (e.g., Bingham, 1922; Hulme, 1974; Moore, 1974). Using Jeffrey's equation, we found that lower slopes result in lower viscosities (all else equal). Therefore, if slope values are underestimated, then we are underestimating the average flow viscosity and our final interpretation of composition.

The yield strength equation (Eq. (3)) uses the average measured slope. Due to data resolution limitations and the inability to observe pre-flow topography, obtaining accurate slope data can be difficult, as outlined by Glaze and Baloga (2007), who used PEDR points for extents far from the lava flow in order to model the topographic variability along those flows. Where using the gridded MOLA data products, sub-kilometer scale surface features are not detectable, and thus do not always correlate with the morphometric data collected for rheologic modeling. The complications with obtaining accurate slope data impact the results of yield strength modeling obtained by the SRA. The higher slope variations result in significant changes in yield strength, with the largest change in slope being over 6 degrees, and the associated change in yield strength being three orders of magnitude between the minimum and maximum calculation. In the case of AM16, the maximum yield strength was an order of magnitude larger than the average yield strength, indicating underestimation could be occurring by utilizing an average slope value in this calculation.

4.2. Topography dataset limitations

The spatial resolution of topographic datasets has a direct effect on our ability to both observe small scale features that could impact flow propagation and the accuracy of the derived slope values. This has routinely been observed in terrestrial remote sensing (Chang and Tsai, 1991; Evans, 1980; Flynn et al., 2023) and to a lesser extent on Mars (Brož et al., 2015; Flynn et al., 2023, Pieterek and Jones, 2024). Flynn et al. (2023) highlighted the 25× difference in measured slope values between a CTX DEM and the MOLA/HRSC DEM, for a channelized lava flow south of Arsia Mons. To further emphasize this point we performed a similar analysis for a lava flow southeast of Elysium Mons using MOLA, HRSC, and CTX DEMs (Fig. 3). The flow was chosen specifically because of the three overlapping topographic datasets.

We followed the same methods as presented in Section 3 for measuring the flow dimensions and followed the SRA modeling approach. The only variation between the two methods is that we used the average slope over the observable flow area from each of the three datasets (Fig. 3). The observable flow length is 31.7 km, the average flow width is 1047 m, and average flow thickness is 24 m. The same trend observed in Flynn et al. (2023) of increasing slope value with increasing spatial resolution is found with the three datasets here (Table 6). Following the methods of the SRA resulted in an effusion rate of 200 m^3/s. The calculated viscosity was 5.7×10^6, 1.5×10^7, and 3.5×10^7 Pa s for the MOLA, HRSC, and CTX DEMs respectively. Calculated yield strengths were 5.7×10^3, 1.5×10^4, and 3.5×10^4 Pa for the MOLA, HRSC, and CTX DEMs respectively. As the spatial resolution of the topographic dataset increased, so did the derived slope values (Table 6), which then resulted in increased viscosity and yield strength. The increased viscosity derived from HRSC and CTX slopes suggests the composition of the flow is more similar to an andesite than a basalt. These results indicate that using MOLA gridded topography underestimates the slope, producing lower viscosity and yield strength modeled values, and thus may provide an inaccurate compositional range for that flow.

All topographic datasets have inherent uncertainty in vertical accuracy. MOLA PEDR data has a 37 cm vertical error (Smith et al., 2003), HRSC and CTX DTMs have a 3 to 5 m vertical uncertainty (Kirk et al., 2021). These vertical uncertainties can affect the measured flow thickness values used in the SRA and the calculated slope data (Millot et al., 2023). The primary objective of this manuscript is specifically on how variations in the measured slope value affect the SRA results. However, it is important to acknowledge the inherent uncertainties in topographic data and how they can affect derived values.

With the increasing abundance of high resolution topographic datasets on Mars these points are of particular importance. As of 2019, CTX-derived DEMs cover ~17 % of the Martian surface. Day et al. (2023) recently published an additional ~1300 CTX and ~ 1300 HiRISE DEMs. HiRISE DEMs do not usually have large enough spatial footprint to cover an entire lava flow but the Colour and Stereo Surface Imaging System (CaSSIS) instrument can generate DEMs with spatial coverage and resolution high enough to observe individual lava flows (Thomas

Table 6
Statistics for slope datasets for Elysium Mons, associated with Fig. 3.

	MOLA	HRSC	CTX
Data Points (count)	312	10,442	213,430
Average Slope (°)	1.36	3.53	8.35
Median Slope (°)	1.37	3.15	7.18
Minimum Slope (°)	0.18	0	0.47
Maximum Slope (°)	2.43	19.14	70.95
Standard Deviation (°)	0.45	2.19	5.03

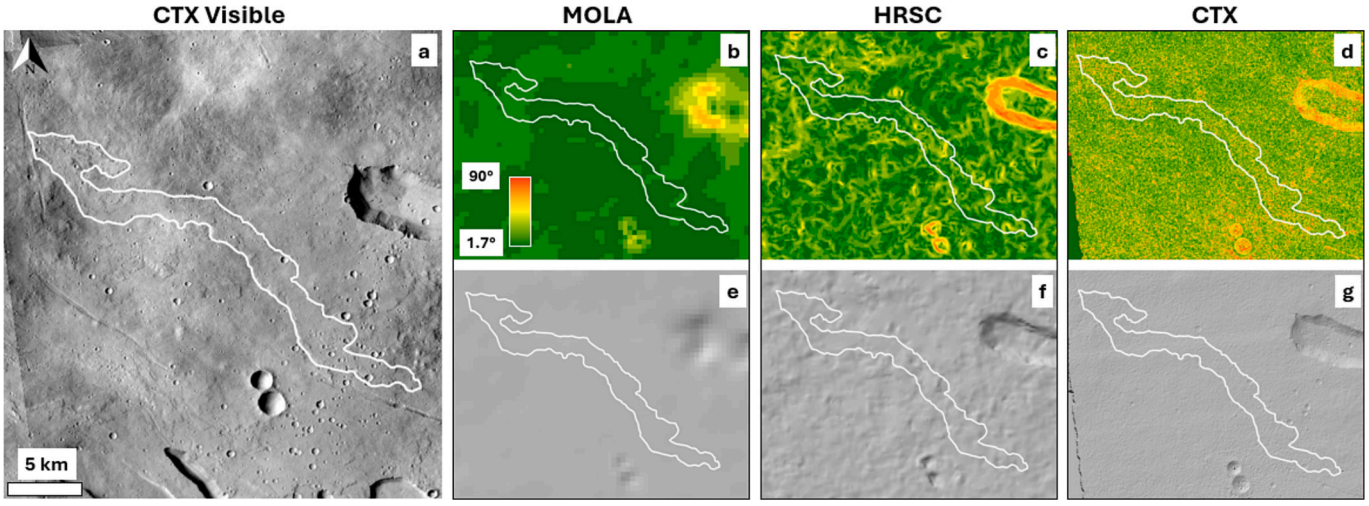

Fig. 3. (a) Lava flow (white outline) southeast of Elysium Mons shown in CTX, (b) MOLA, (c) HRSC, and (d) CTX derived slope data as well as the corresponding elevation hillshade images for MOLA (e), HRSC (f), and CTX (g), respectively. Statistics for each of the slope dataset are in Table 6.

et al., 2017). These high resolution DEMs do not currently have global coverage, however they should be leveraged where possible for lava flow modeling. Our results directly show the importance of using the highest topographic data available, which can significantly impact the interpretation of lava flow rheology and composition. If high resolution DEMs are unavailable, then interpreting model results should be done with caution.

5. Conclusions

Several prior studies modeling the emplacement of Martian lava flows have used measured flow dimensions and the SRA approach to calculate flow rheology and emplacement conditions (e.g., Hiesinger et al., 2007; Pasckert et al., 2012; Peters et al., 2021; Wiedeking et al., 2022). In this study, we investigated specifically how variations in the measured slope used in the SRA affects the calculated values, namely the viscosity and yield strength. To assess this we investigated sixteen flows, fourteen south and two north of Arsia Mons. The results indicate that the variations and uncertainty in the slope value results in a 60 % and 70 % change in the calculated viscosity and yield strength, respectively. Based on the viscosity, this can then lead to an inaccurate lava composition assigned to that flow. Furthermore, we highlight that using the standard deviation of the average slope is more representative of the measured values rather than the previously used percent-based methods.

In addition to the assessment of how variations in the measured slope affect the results from the SRA, we highlight how increased spatial resolution topographic datasets, and by extension, calculated slope affect the modeled results as well. The results show that increased spatial resolution of topographic data produces an increase in the calculated viscosity and yield strength. Although moderate to high resolution digital topographic data are not globally available on Mars, these results emphasize the need to incorporate it where possible to reduce the biases from lower resolution datasets.

Future studies modeling Martian lava flows that utilize the SRA should consider how the input slope value is derived, incorporate higher resolution topography if available, and acknowledge the assumptions and limitations of using low resolution topographic datasets.

CRediT authorship contribution statement

Frances P. Russo: Writing – original draft, Visualization, Investigation, Formal analysis, Data curation. **Ian T.W. Flynn:** Writing – review & editing, Visualization, Validation, Supervision, Methodology, Investigation, Formal analysis, Conceptualization. **Sean I. Peters:** Writing – original draft, Validation. **Michael S. Ramsey:** Writing – review & editing, Supervision, Resources, Project administration, Funding acquisition.

Declaration of competing interest

The authors declare that they have no known competing financial interests or personal relationships that could have appeared to influence the work reported in this paper.

Acknowledgments

This undergraduate student work was supported by a NASA Solar System Workings (SSW) grant 80NSSC19K0547 to MSR.

Data availability

All flow measurements and modeling results from the study are available via Flynn (2025).

References

Baloga, S.M., Glaze, L.S., 2008. A self-replication model for long channelized lava flows on the Mars plains. J. Geophys. Res. E Planets 113 (5), 1–15. https://doi.org/10.1029/2007JE002954.

Belousov, A., Belousova, M., 2017. Dynamics and viscosity of 'a'a and pahoehoe lava flows of the 2012–2013 eruption of Tolbachik volcano, Kamchatka (Russia). Bull. Volcanol. 80 (1). https://doi.org/10.1007/s00445-017-1180-2.

Berman, D.C., Crown, D.A., 2019. Chronology of volcanism in southern tharsis, Mars: Constraints from lava flows in daedalia planum. In: 46th Lunar and Planetary Science Conference.

Bingham, E.C., 1922. Fluidity and Plasticity. McGraw-Hill, N.Y, p. 440.

Bleacher, J.E., Greeley, R., Williams, D.A., Cave, S.R., Neukum, G., 2007. Trends in effusive style at the Tharsis Montes, Mars, and implications for the development of the Tharsis province. J. Geophys. Res. E Planets 112 (9), 1–15. https://doi.org/10.1029/2006JE002873.

Bonny, E., Wright, R., 2017. Predicting the end of lava flow-forming eruptions from space. Bull. Volcanol. 79, 52. https://doi.org/10.1007/s00445-017-1134-8.

Brož, P., Cadek, O., Hauber, E., Rossi, A.P., 2015. Scoria cones on Mars: detailed investigation of morphometry based on high-resolution digital elevation models. J. Geophys. Res. Planets 175 (4449), 238. https://doi.org/10.1038/175238c0.

Carr, M.H., 1973. Volcanism on mars. J. Geophys. Res. 78 (20), 4049–4062.

Chang, K.T., Tsai, B.W., 1991. The effect of dem resolution on slope and aspect mapping. Cartogr. Geogr. Inf. Syst. 18 (1), 69–77. https://doi.org/10.1559/152304091783805626.

Chevrel, M.O., Platz, T., Hauber, E., Baratoux, D., Lavallée, Y., Dingwell, D.B., 2013. Lava flow rheology: a comparison of morphological and petrological methods. Earth Planet. Sci. Lett. 384, 109–120. https://doi.org/10.1016/j.epsl.2013.09.022.

Chevrel, M., Harris, A.J.L., Rowland, S.K., 2018. Computers and geosciences PyFLOWGO: an open-source platform for simulation of channelized lava thermo-rheological properties, 111 (November 2017), 167–180. https://doi.org/10.1016/j.cageo.2017.11.009.

Cigolini, C., Borgia, A., Casertano, L., 1984. Intra-crater activity, aa-block lava, viscosity and flow dynamics: Arenal volcano, Costa Rica. J. Volcanol. Geotherm. Res. 20 (1–2), 155–176.

Crown, D.A., Ramsey, M.S., 2017. Morphologic and thermophysical characteristics of lava flows southwest of Arsia Mons, Mars. J. Volcanol. Geotherm. Res. 342, 13–28. https://doi.org/10.1016/j.jvolgeores.2016.07.008.

Crown, D.A., Berman, D.C., Rams, 2015. Lava flow fields of Southern Tharsis, Mars: flow types, interactions, and ages. In: 46th Lunar and Planetary Science Conference, 1439, pp. 2–3. https://doi.org/10.1029/2006JE002873.

Day, M., Kim, E., Sullivan, M., Goudge, T., Paige, D., 2023. High Resolution DEMs for Mars: A repository of paired HiRISE and CTX DEMs. In: 6th Planetary Data Workshop, Flagstaff, Arizona.

Evans, I.S., 1980. An integrated system of terrain analysis and slope mapping. Zeitschrift Fur Geomorphologie 36, 274–295.

Fergason, R.L., Hare, T.M., Laura, J., 2018. HRSC and MOLA Blended Digital Elevation Model at 200m v2, Astrogeology PDS Annex. US Geological Survey.

Flynn, I., 2025. In: SRA Data For Russo, et al. (Eds.), Data Set. Zenodo. https://doi.org/10.5281/zenodo.14852236.

Flynn, I.T.W., Crown, D.A., Ramsey, M.S., 2022. Determining emplacement conditions and vent locations for channelized lava flows southwest of Arsia Mons. J. Geophys. Res. Planets 127 (11). https://doi.org/10.1029/2022JE007467.

Flynn, I.T.W., Chevrel, M.O., Crown, D.A., Ramsey, M.S., 2023. The effects of digital elevation model resolution on the PyFLOWGOthermorheological lava flow model. Environ. Model Softw. 167, 105768. https://doi.org/10.1016/j.envsoft.2023.105768.

Ganesh, I., Carter, L.M., Smith, I.B., 2020. SHARAD mapping of Arsia Mons caldera. J. Volcanol. Geotherm. Res. 390. https://doi.org/10.1016/j.jvolgeores.2019.106748.

Gansecki, C., Lopaka Lee, R., Shea, T., Lundblad, S.P., Hon, K., Parcheta, C., 2019. The tangled tale of Kīlauea's 2018 eruption as told by geochemical monitoring. Science 366 (6470). https://doi.org/10.1126/science.aaz0147.

Glaze, L.S., Baloga, S.M., 2007. Topographic variability on Mars: implications for lava flow modeling. J. Geophys. Res. E Planets 112 (8), 1–9. https://doi.org/10.1029/2006JE002879.

Gregg, T.K.P., 2017. Patterns and processes: subaerial lava flow morphologies: a review. J. Volcanol. Geotherm. Res. 342, 3–12. https://doi.org/10.1016/j.jvolgeores.2017.04.022.

Gregg, T.K.P., Fink, J.H., 2000. A laboratory investigation into the effects of slope on lava flow morphology. J. Volcanol. Geotherm. Res. 96 (3–4), 145–159. https://doi.org/10.1016/S0377-0273(99)00148-1.

Harris, A., Murray, J.B., Aries, S.E., Davies, M.A., Flynn, L.P., Wooster, M.J., et al., 2000. Effusion rate trends at Etna and Krafla and their implications for eruptive mechanisms. J. Volcanol. Geotherm. Res. 102 (3–4), 237–269. https://doi.org/10.1016/S0377-0273(00)00190-6.

Hiesinger, H., Head, I.W., Neukum, G., 2007. Young lava flows on the eastern flank of Ascaraeus Mons: rheological properties derived from high resolution stereo camera (HRSC) images and Mars orbiter laser altimeter(MOLA) data. J. Geophys. Res. E Planets 112 (5). https://doi.org/10.1029/2006JE002717.

Hulme, G., 1974. The interpretation of lava flow morphology. Geophys. J. R. Astron. Soc. 39, 361–383.

Kerr, R.C., Griffiths, R.W., Cashman, K., v., 2006. Formation of channelized lava flows on an unconfined slope. J. Geophys. Res. Solid Earth 111 (10), 1–13. https://doi.org/10.1029/2005JB004225.

Kirk, R.L., Mayer, D.P., Fergason, R.L., Redding, B.L., Galuszka, D.M., Hare, T.M., Gwinner, K., 2021. Evaluating stereo digital terrain model quality at mars rover landing sites with hrsc, ctx, and hirise images. Remote Sens. 13 (17). https://doi.org/10.3390/rs13173511.

Kolzenburg, S., Jaenicke, J., Münzer, U., Dingwell, D.B., 2018. The effect of inflation on the morphology-derived rheological parameters of lava flows and its implications for interpreting remote sensing data - A case study on the 2014/2015 eruption at Holuhraun, Iceland. J. Volcanol. Geotherm. Res. 357, 200–212. https://doi.org/10.1016/j.jvolgeores.2018.04.024.

Malin, M.C., Bell III, J.F.M., Cantor, B.A., Caplinger, M.A., Calvin, W.M., Clancy, R.T., Edgett, K.S., Edwards, L., Haberle, R.M., James, P.B., Lee, S.W., Ravine, M.A., Thomas, P.C., Wolff, M.J., 2007. Context camera investigation onboard the Mars Reconaissance orbiter. J. Geophys. Res. 112, E05504. https://doi.org/10.1029/2006JE002808.

Millot, C., Quantin-Nataf, C., Leyrat, C., Lherm, V., Volat, M., 2023. Assessing slope uncertainties of martian Digital Elevation Models from numerical propagation of errors on synthetic geological surfaces. Icarus 391. https://doi.org/10.1016/j.icarus.2022.115341.

Moore, H.J., 1974. A note on the Imbriu flows and Bingham plastics. In: U.S. Geological Survey Professional Paper, 900, p. 29.

Mouginis-Mark, P., Yoshioka, M.T., 1998. The long lava flows of Elysium Planita, Mars. J. Geophys. Res. Planets 103 (E8), 19389–19400.

Mouginis-Mark, P.J., Rowland, S.K., 2008. Lava flows at Arsia Mons, Mars: insights from a graben imaged by HiRISE. Icarus 198 (1), 27–36. https://doi.org/10.1016/j.icarus.2008.06.015.

Murase, T., McBirney, A.R., 1973. Properties of some common igneous rocks and their melts at high temperatures. Geol. Soc. Am. Bull. 84 (11), 3563–3592.

Pasckert, J.H., Hiesinger, H., Reiss, D., 2012. Rheologies and ages of lava flows on Elysium Mons, Mars. Icarus 219 (1), 443–457. https://doi.org/10.1016/j.icarus.2012.03.014.

Pedersen, G.B.M., Belart, J.M.C., Óskarsson, B.V., Gudmundsson, M.T., Gies, N., Högnadóttir, T., Hjartardóttir, Á.R., Pinel, V., Berthier, E., Dürig, T., Reynolds, H.I., Hamilton, C.W., Valsson, G., Einarsson, P., Ben-Yehosua, D., Gunnarsson, A., Oddsson, B., 2022. Volume, effusion rate, and lava transport during the 2021 Fagradalsfjall eruption: results from near real-time photogrammetric monitoring. Geophys. Res. Lett. 49 (13). https://doi.org/10.1029/2021GL097125.

Peitersen, M., Crown, D., 1999. Downflow flows width behavior of Martian and terrestrial lava flows. J. Geophys. Res. 104, 8473–8488.

Peters, S.I., Christensen, P.R., Clarke, A.B., 2021. Lava flow eruption conditions in the Tharsis Volcanic Province on Mars. J. Geophys. Res. Planets 126 (n/a). https://doi.org/10.1029/2020JE006791 e2020JE006791.

Pieterek, B., Jones, T.J., 2024. Mildly explosive eruptions at Martian low-shield volcanoes. Commun. Earth Environ. 5, 542. https://doi.org/10.1038/s43247-024-01697-w.

Pinkerton, H., 1987. Factors affecting the morphology of lava flows. Endeavour N. S. 11 (2), 73–79.

Pinkerton, H., Sparks, R.S.J., 1976. The 1975 sub-terminal lavas, Mount Etna: a case history of the formation of a compound lava field. J. Volcanol. Geotherm. Res. 1 (2), 167–182.

Ramsey, M.S., Harris, A.J.L., Crown, D.A., 2016. What can thermal infrared remote sensing of terrestrial volcanoes tell us about processes past and present on Mars? J. Volcanol. Geotherm. Res. 311, 198–216. https://doi.org/10.1016/j.jvolgeores.2016.01.012.

Ramsey, M.S., Chevrel, M.O., Coppola, D., Harris, A.J.L., 2019. The influence of emissivity on the thermo-rheological modeling of the channelized lava flows at tolbachik volcano. Annals of Geophys. 62 (2 Special Issue). https://doi.org/10.4401/ag-8077.

Richardson, J.A., Wilson, J.A., Connor, C.B., Bleacher, J.E., Kiyosugi, K., 2017. Recurrence rate and magma effusion rate for the latest volcanism on Arsia Mons, Mars. Earth Planet. Sci. Lett. 458, 170–178. https://doi.org/10.1016/j.epsl.2016.10.040.

Rowland, S.K., Garbeil, H., Harris, A.J.L., 2005. Lengths and hazards from channel-fed lava flows on Mauna Loa, Hawai'i, determined from thermal and downslope modeling with FLOWGO. Bull. Volcanol. 67 (7), 634–647. https://doi.org/10.1007/s00445-004-0399-x.

Smith, D.E., Zuber, M.T., Neumann, G.A., Guinness, E.A., Slavney, S., 2003. Mars Global Surveyor laser altimeter Mission Experiment Gridded Data Record, MGS-M-MOLA-5-MEGDR-L3-V1.0 [Data set]. NASA Planetary Data System. https://doi.org/10.17189/1519460.

Soldati, A., Harris, A.J.L., Gurioli, L., Villeneuve, N., Rhéty, M., Gomez, F., Whittington, A., 2018. Textural, thermal, and topographic constraints on lava flow system structure: the December 2010 eruption of piton de la Fournaise. Bull. Volcanol. 80 (10). https://doi.org/10.1007/s00445-018-1246-9.

Sparks, R.S.J., Pinkerton, H., Hulme, G., 1976. Classification and formation of lava levees on Mount Etna, Sicily. Geology 4 (5), 269–271.

Staudacher, T., Ferrazzini, V., Peltier, A., Kowalski, P., Boissier, P., Catherine, P., Lauret, F., Massin, F., 2009. The April 2007 eruption and the Dolomieu crater collapse, two major events at piton de la Fournaise (La Réunion Island, Indian Ocean). J. Volcanol. Geotherm. Res. 184 (1–2), 126–137. https://doi.org/10.1016/j.jvolgeores.2008.11.005.

Tanaka, K.L., Robbins, S.J., Fortezzo, C.M., Skinner, J.A., Hare, T.M., 2014. The digital global geologic map of Mars: chronostratigraphic ages, topographic and crater morphologic characteristics, and updated resurfacing history. Planet. Space Sci. 95, 11–24. https://doi.org/10.1016/j.pss.2013.03.006.

Theilig, E., Greeley, R., 1986. Lava flows on Mars: analysis of small surface features and comparisons with terrestrial analogs. J. Geophys. Res. 91 (B13), E193. https://doi.org/10.1029/jb091ib13p0e193.

Thomas, N., Cremonese, G., Ziethe, R., Gerber, M., Brändli, M., Bruno, G., Erismann, M., Gambicorti, L., Gerber, T., Ghose, K., Gruber, M., Gubler, P., Mischler, H., Jost, J., Piazza, D., Pommerol, A., Rieder, M., Roloff, V., Servonet, A., Wray, J.J., 2017. The colour and stereo surface imaging system (CaSSIS) for the ExoMars trace gas orbiter. Space Sci. Rev. 212 (3–4), 1897–1944. Springer Netherlands. https://doi.org/10.1007/s11214-017-0421-1.

Vetere, F., Behrens, H., Holtz, F., Neuville, D.R., 2006. Viscosity of andesitic melts—new experimental data and a revised calculation model. Chem. Geol. 228 (4), 233–245.

Voigt, J.R.C., Hamilton, C.W., Steinbrügge, G., Höskuldsson, Á., Jónsdottir, I., Thordarson, T., 2022. Linking lava morphologies to effusion rates for the 2014–2015 Holuhraun lava flow field, Iceland. Geology 50 (1), 71–75. https://doi.org/10.1130/G49251.1.

Voigt, J.R.C., Hamilton, C.W., Steinbrügge, G., Christoffersen, M.S., Nerozzi, S., Kerber, L., Holt, J.W., Carter, L.M., 2023. Revealing Elysium Planitia's young geologic history: constraints on lava emplacement, areas, and volumes. J. Geophys. Res. Planets 128 (12). https://doi.org/10.1029/2023JE007947.

Wadge, G., 1981. The variation of magma discharge during basaltic eruptions. J. Volcanol. Geotherm. Res. 11, 139–168.

Warner, N.H., Gregg, T.K.P., 2003. Evolved lavas on Mars? Observations from southwest Arsia Mons and Sabancaya volcano, Peru. J. Geophys. Res. E Planets 108 (10). https://doi.org/10.1029/2002je001969.

Werner, S.C., 2009. The global martian volcanic evolutionary history. Icarus 201 (1), 44–68. https://doi.org/10.1016/j.icarus.2008.12.019.

Wiedeking, S., Lentz, A., Pasckert, J.H., Raack, J., Schmedemann, N., Hiesinger, H., 2022. Rheological properties and ages of lava flows on Alba Mons, Mars. Icarus 389, 115267. https://doi.org/10.1016/j.icarus.2022.115267.

Wilson, L., Head, J.W., 1983. A comparison of volcanic eruption processes on Earth, Moon, Mars, Io and Venus. Nature 302 (5910), 663–669. https://doi.org/10.1038/302663a0.

Zimbelman, J.R., Garry, W.B., Bleacher, J.E., Crown, D.A., 2015. Volcanism on Mars. In: *The Encyclopedia of Volcanoes*. Elsevier, pp. 717–728. https://doi.org/10.1016/B978-0-12-385938-9.00041-9.